Global Biogeochemical Cycles

RESEARCH ARTICLE
10.1029/2020GB006887

Nitrate Supply Routes and Impact of Internal Cycling in the North Atlantic Ocean Inferred From Nitrate Isotopic Composition

F. Deman[1,2], D. Fonseca-Batista[1,3], A. Roukaerts[1], M. I. García-Ibáñez[4], E. Le Roy[5], E. P. D. N. Thilakarathne[1,6], M. Elskens[1], F. Dehairs[1], and F. Fripiat[7]

[1]Analytical, Environmental, and Geochemistry, Earth System Sciences Research Group, Vrije Universiteit Brussel, Brussels, Belgium, [2]Unité d'Océanographie Chimique, Freshwater and Oceanic Science Unit of Research, Université de Liège, Liège, Belgium, [3]Department of Biology, Dalhousie University, Halifax, Nova Scotia, Canada, [4]Instituto de Investigaciones Marinas, IIM-CSIC, Vigo, Spain, [5]Department of Marine Chemistry and Geochemistry, Woods Hole Oceanographic Institution, Woods Hole, MA, USA, [6]Department of Animal Science, Uva Wellassa University, Badulla, Sri Lanka, [7]Department of Geosciences, Environment and Society, Université libre de Bruxelles, Brussels, Belgium

Key Points:

- Nitrate assimilation controls the nitrate isotopic composition in surface waters of the North Atlantic subpolar gyre
- Nitrate isotopic composition reveals that nitrate is supplied from subpolar to subtropical gyre by Ekman transport and isopycnal mixing
- N_2 fixation and Mediterranean outflow have an impact on nitrate isotopic composition in the North Atlantic Ocean

Supporting Information:

Supporting Information may be found in the online version of this article.

Correspondence to:

F. Deman,
florian.deman@vub.be

Citation:

Deman, F., Fonseca-Batista, D., Roukaerts, A., García-Ibáñez, M. I., Le Roy, E., Thilakarathne, E. P. D. N., et al. (2021). Nitrate supply routes and impact of internal cycling in the North Atlantic Ocean inferred from nitrate isotopic composition. *Global Biogeochemical Cycles*, *35*, e2020GB006887. https://doi.org/10.1029/2020GB006887

Received 12 NOV 2020
Accepted 19 MAR 2021

Abstract In this study we report full-depth water column profiles for nitrogen and oxygen isotopic composition ($\delta^{15}N$ and $\delta^{18}O$) of nitrate (NO_3^-) during the GEOTRACES GA01 cruise (2014). This transect intersects the double gyre system of the subtropical and subpolar regions of the North Atlantic separated by a strong transition zone, the North Atlantic Current. The distribution of NO_3^- $\delta^{15}N$ and $\delta^{18}O$ shows that assimilation by phytoplankton is the main process controlling the NO_3^- isotopic composition in the upper 150 m, with values increasing in a NO_3^- $\delta^{18}O$ versus $\delta^{15}N$ space along a line with a slope of one toward the surface. In the subpolar gyre, a single relationship between the degree of NO_3^- consumption and residual NO_3^- $\delta^{15}N$ supports the view that NO_3^- is supplied via Ekman upwelling and deep winter convection, and progressively consumed during the Ekman transport of surface water southward. The co-occurrence of partial NO_3^- assimilation and nitrification in the deep mixed layer of the subpolar gyre elevates subsurface NO_3^- $\delta^{18}O$ in comparison to deep oceanic values. This signal propagates through isopycnal exchanges to greater depths at lower latitudes. With recirculation in the subtropical gyre, cycles of quantitative consumption-nitrification progressively decrease subsurface NO_3^- $\delta^{18}O$ toward the $\delta^{18}O$ of regenerated NO_3^-. The low NO_3^- $\delta^{15}N$ observed south of the Subarctic Front is mostly explained by N_2 fixation, although a contribution from the Mediterranean outflow is required to explain the lower NO_3^- $\delta^{15}N$ signal observed between 600 and 1500 m depth close to the Iberian margin.

1. Introduction

The biological carbon pump plays a crucial role in the regulation of Earth's climate and the distribution of biogeochemical properties in the ocean, by exporting to the deep ocean CO_2 that is fixed into biomass during photosynthesis in the sunlit surface layer, through the sinking of particles and their subsequent remineralization. Phytoplankton requires macro-nutrients for the synthesis of organic matter. Nitrogen (N) is considered as one of the most important nutrients since it limits productivity in many oceanic regions (Moore et al., 2013). The North Atlantic Ocean, which hosts one of the most productive spring phytoplankton blooms of the world's ocean (Longhurst, 2007), is estimated to be a significant contributor to the global oceanic export production (Falkowski et al., 1998; Sanders et al., 2014).

The North Atlantic Ocean is characterized by the classical double gyre system of the subtropical and subpolar gyres (Figure 1). Both gyres harbor contrasting physical and biogeochemical features (Sanders et al., 2014) and are separated by a strong transition area, the North Atlantic Current (NAC). In addition, the Atlantic Meridional Overturning Circulation is a key component of the Earth's climate system, with the NAC carrying a northward flow of warm and salty waters balanced by a southward flow of colder deep waters (North Atlantic Deep Water) (Buckley & Marshall, 2016). The North Atlantic subtropical gyre is considered to be a year-round stratified oligotrophic N-limited area (Moore et al., 2008, 2013), where N_2 fixation performed by diazotrophs plays an important role in providing fixed N (or bioavailable N) to the surface waters (Capone et al., 2005, 2008). In contrast, a strong seasonality is observed in the North Atlantic subpolar gyre. The relief of winter light limitation induces the onset of a spring phytoplankton bloom supported by

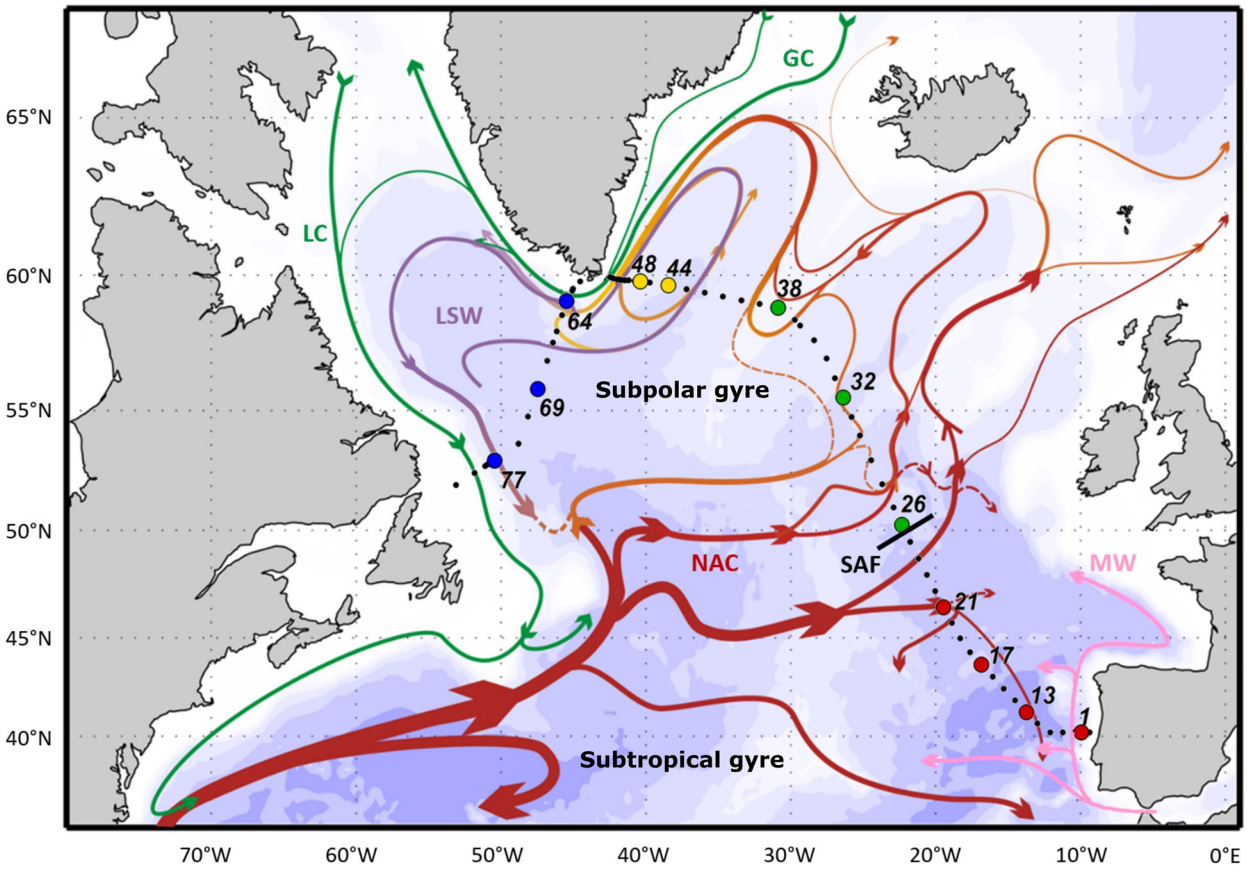

Figure 1. Sampling locations (n = 78; dots) of the GEOTRACES GA01 (GEOVIDE) cruise along the OVIDE transect in the North Atlantic (from the Iberian margin to Greenland) and in the Labrador Sea (from Greenland to Newfoundland) with a simplified schematic of the circulation (adapted from Daniault et al., 2016). Selected stations for nitrate isotopic composition are represented by colored dots (n = 12; labeled with station number), with colors referring to the studied regions: South of Subarctic Front (SAF; red), Iceland basin (green), Irminger basin (yellow) and Labrador basin (blue). The approximate position of the SAF (50°N; Zunino et al., 2017) is represented by the black bar, while arrows represent the main surface currents (North Atlantic Current [NAC], Greenland Current [GC] and Labrador current [LC]). Intermediate water masses discussed in this study are also represented: Labrador Seawater (LSW) and Mediterranean Water (MW).

nutrients supplied through deep winter convection and leads to a strong pulse in export production (Follows & Dutkiewicz, 2002; Harrison et al., 2013; Henson et al., 2009; Martin et al., 2011).

The oceanic inventory of fixed N is set by both inputs (mostly N_2 fixation) and outputs (mostly sedimentary and water-column denitrification) (Deutsch et al., 2007; DeVries et al., 2013; Gruber & Galloway, 2008). Within the ocean, the distribution of N into the different pools is controlled by oceanic circulation and internal cycle processes such as assimilation, remineralization (i.e., particulate N to ammonium) and nitrification (i.e., ammonium to nitrate). The majority of fixed N exists in the form of nitrate (NO_3^-) and the coupled nitrogen ($\delta^{15}N$) and oxygen ($\delta^{18}O$) isotopic composition is a powerful tool to study both the oceanic budget and the internal cycling ($\delta^{15}N = (({}^{15}N/{}^{14}N)_{sample}/({}^{15}N/{}^{14}N)_{reference}\text{-}1)$, expressed in ‰ with atmospheric N_2 as the reference; $\delta^{18}O = (({}^{18}O/{}^{16}O)_{sample}/({}^{18}O/{}^{16}O)_{reference}\text{-}1)$, expressed in ‰ with Vienna Standard Mean Ocean Water (VSMOW) as the reference). Measurable changes in NO_3^- $\delta^{15}N$ and NO_3^- $\delta^{18}O$ are induced by N transformations that occur with different degrees of kinetic fractionation. The latter are expressed as isotope effects (ε) defined by the ratio of reaction rates at which the two isotopes are converted from reactant to product (i.e., ${}^{15}\varepsilon$ (‰) = (1-(${}^{15}k/{}^{14}k$)) for N and ${}^{18}\varepsilon$ (‰) = (1-(${}^{18}k/{}^{16}k$)) for O, where ${}^{x}k$ is the conversion rate coefficient for the ${}^{x}N$ or ${}^{x}O$-containing reactant).

NO_3^- isotopic measurements are still scarce and only a few studies have been performed in the subpolar and inter-gyre regions of the North Atlantic Ocean (Marconi et al., 2017, 2019; Peng et al., 2018; Van Oostende et al., 2017). In the present study we report full-depth water column profiles for nitrogen and oxygen

isotopic composition of NO_3^- along the GEOTRACES GA01 transect (hereafter referred to as GEOVIDE). The main objectives are to understand (i) how NO_3^- is supplied into and exchanged between the subpolar and subtropical gyres, and (ii) the impacts of biological activity such as NO_3^- assimilation, N_2 fixation and remineralization-nitrification on the NO_3^- pool.

2. Material and Methods

The GEOVIDE cruise took place from May 15 to June 30, 2014 on board the R/V *"Pourquoi pas?"* along the OVIDE transect in the North Atlantic Ocean (from the Iberian margin to Greenland) and across the Labrador Sea (from Greenland to Newfoundland) (Figure 1; see also Sarthou et al., 2018). The complete water column was sampled at 78 stations using a rosette equipped with a SBE 911 CTD and 24 Niskin bottles. Temperature, salinity, and oxygen were measured from surface to bottom while seawater samples for biogeochemical measurements were collected from bottom to surface during the first deployment of the rosette (Lherminier & Sarthou, 2017; Zunino et al., 2017). Additional samples were collected during a subsequent rosette deployment to achieve a greater vertical resolution in the upper 200 m of the water column (see supporting information Table S1).

At each station, concentrations of nitrite ($[NO_2^-]$) and nitrate ($[NO_3^-]$ being calculated from $([NO_3^-]+[NO_2^-]) - [NO_2^-]$) of the full-depth water column samples were analyzed onboard using a Seal Analytical AutoAnalyser III and standard colorimetric methods (Grasshoff et al., 1999; Perez et al., 2018). Additional samples from the subsequent rosette deployment (upper 200 m) were filtered (Acrodiscs; 0.2 μm porosity) and stored at −20°C for nutrient analysis at the home-based laboratory (AMGC, VUB, Brussels, Belgium) using a Seal Analytical QuAAtro39 and the same standard colorimetric methods. The standard deviation and detection limit for $[NO_3^-]$ were 100 and 90 nmol l^{-1}, respectively (Fonseca-Batista et al., 2019; García-Ibáñez et al., 2018).

Nitrate isotope samples were collected throughout the depth of the water column at 12 selected stations (Figure 1). Seawater was filtered (Acrodiscs; 0.2 μm porosity), stored in HDPE bottles pre-rinsed with sample water and kept frozen at −20°C until analysis. At the home-based laboratory, NO_3^- $\delta^{15}N$ and $\delta^{18}O$ were determined for all samples with $[NO_3^-] \geq 2$ μmol l^{-1}, using the denitrifier method (Casciotti et al., 2002; Sigman et al., 2001). Briefly, denitrifying bacteria (*Pseudomonas chlororaphis* ssp. *aureofaciens*) were used to quantitatively reduce 20 or 30 nmol of NO_3^- into N_2O prior to measurement by gas chromatography/isotope ratio mass spectrometry (GC/IRMS, Thermo DeltaV), using a custom-build "purge and cryo-trap" system similar to the one described by Casciotti et al. (2002). Measurements were referenced to atmospheric N_2 (for $\delta^{15}N$) and VSMOW (for $\delta^{18}O$) using international NO_3^- certified reference materials: IAEA-N3 ($\delta^{15}N = +4.7$‰; $\delta^{18}O = +25.6$‰) and USGS-34 ($\delta^{15}N = -1$‰; $\delta^{18}O = -27.9$‰) (Böhlke et al., 2003; Gonfiantini et al., 1995). Nitrite (NO_2^-) was removed from the samples by reaction with sulfamic acid prior to the NO_3^- isotope analyses to avoid any interference with NO_3^- (Granger & Sigman, 2009). Sulfamic acid was also applied to NO_3^- certified reference materials to ensure that no contamination originated from this treatment. Since measurements of NO_3^- $\delta^{18}O$ are sensitive to NO_3^- concentration (Weigand et al., 2016), NO_3^- reference materials were diluted using low-nutrient Sargasso Sea surface water to generate standards with concentrations that bracket the ones of the samples. Any trend between the measured NO_3^- $\delta^{18}O$ of the two certified reference materials bracketing the concentrations of the samples were used to generate a linear regression to correct for any concentration effect (Marconi et al., 2015; Weigand et al., 2016). Samples ($n = 302$) were analyzed in duplicate, yielding median standard deviation values (1 SD) of 0.13‰ and 0.25‰ for NO_3^- $\delta^{15}N$ and $\delta^{18}O$, respectively (see supporting information Table S1). Previous studies in the subtropical gyres corrected for the effect of salinity-driven depth variation in the $\delta^{18}O$ of seawater on NO_3^- $\delta^{18}O$ (Fawcett et al., 2015; Knapp et al., 2008), using a linear relationship between salinity and $\delta^{18}O$ of ambient seawater (Bigg & Rohling, 2000) and assuming that most of the NO_3^- is nitrified in situ (i.e., NO_3^- $\delta^{18}O$ being set by H_2O $\delta^{18}O + 1.1$‰). Given the much smaller variations in salinity in our study (i.e., 0.3), this correction (i.e., 0.17‰) is below our precision for NO_3^- $\delta^{18}O$ and is, therefore, not considered further.

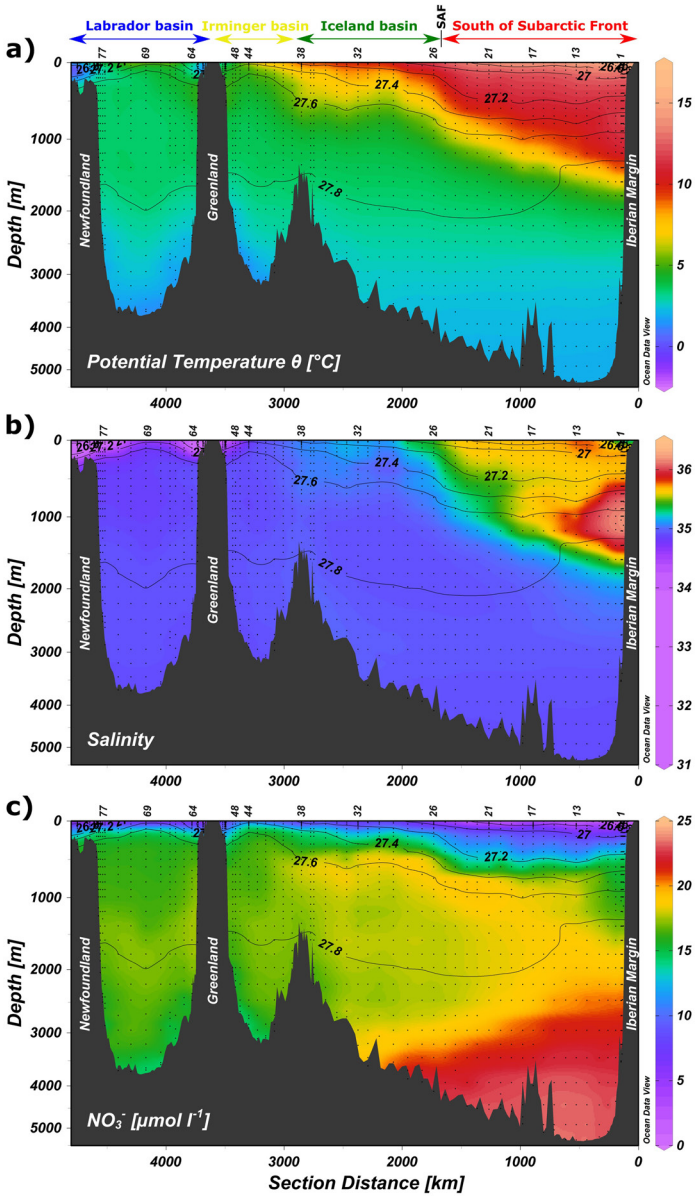

Figure 2. Full depth water column profiles of observed (a) potential temperature (θ; °C), (b) salinity, and (c) nitrate concentration (µmol l^{-1}), overlaid by black contours of potential density anomaly at 0 dbar (σ_0; kg m^{-3}). Colored arrows above the panels indicate the four studied regions as in Figure 1: South of Subarctic Front (red), Iceland basin (green), Irminger basin (yellow) and Labrador basin (blue).

3. Results

The Subarctic Front (SAF), roughly centered around 50°N and associated with the central branch of the NAC, separates colder and fresher waters of the subpolar gyre from warmer and saltier waters of the subtropical gyre (Figures 2a and 2b), characterized by a counter-clockwise and clockwise circulation, respectively (Daniault et al., 2016; Rossby, 1996; Zunino et al., 2017). These two gyres have contrasting biogeochemical and physical properties, with the subpolar gyre being well ventilated with nutrient-rich deep ocean waters due to winter vertical mixing and Ekman upwelling, and the subtropical gyre having low-nutrient surface waters which are isolated from the deep ocean by a permanent thermocline (Figure 2c). The GEOVIDE hydrographic transect intersects different regions of the North Atlantic Ocean (Figure 1): the subtropical gyre south of the SAF (stations 1, 13, 17, and 21; red) and the subpolar gyre north of the SAF

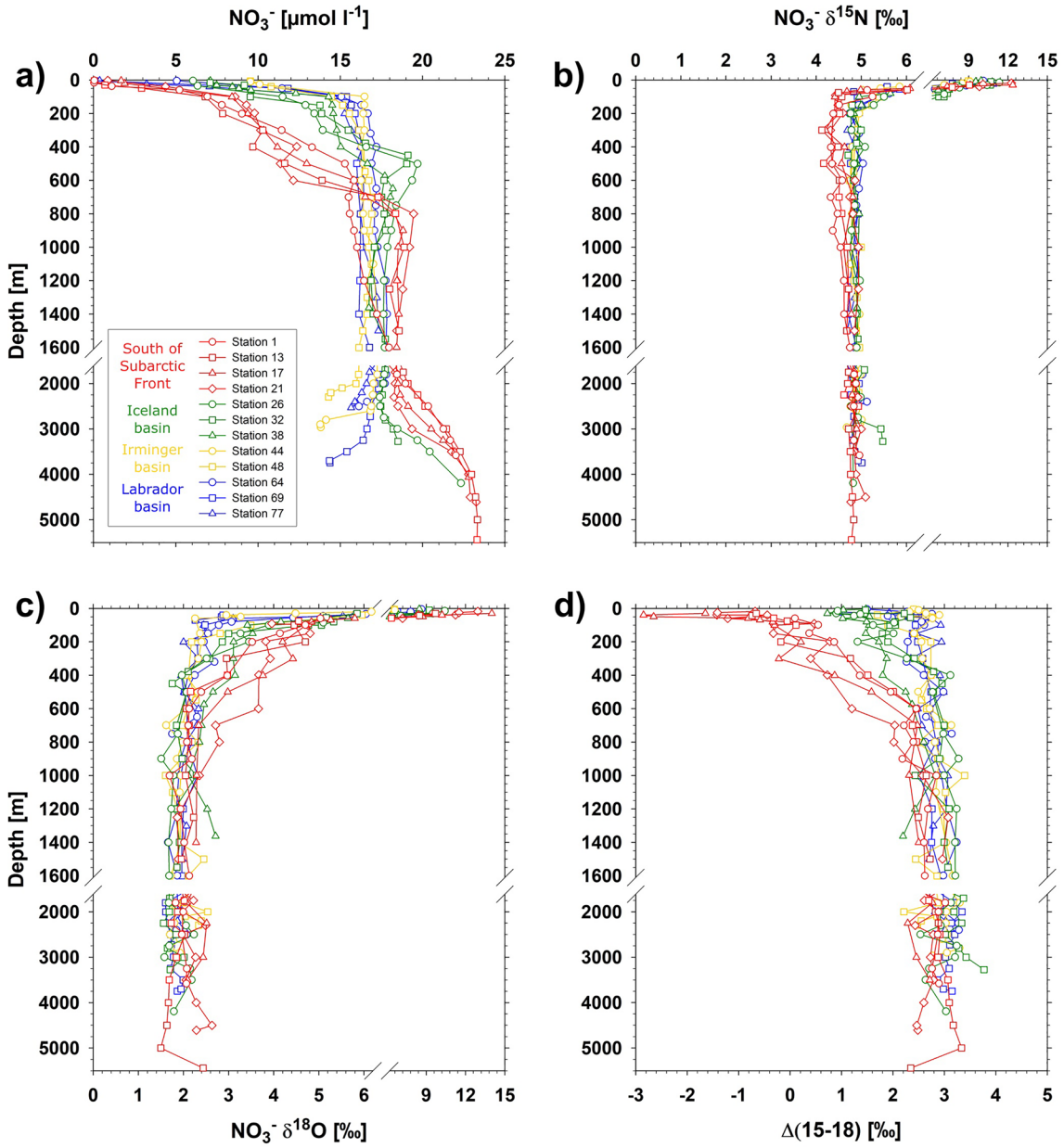

Figure 3. Depth profiles of observed (a) nitrate concentration (NO_3^-; µmol l^{-1}), (b) NO_3^- $\delta^{15}N$ (‰), (c) NO_3^- $\delta^{18}O$ (‰) and (d) Δ(15–18) (‰). Colors refer to the four studied regions as in Figure 1: South of Subarctic Front (red), Iceland basin (green), Irminger basin (yellow) and Labrador basin (blue).

comprising the Iceland basin (stations 26, 32, and 38; green), the Irminger basin (stations 44 and 48; yellow) and the Labrador basin (stations 64, 69, and 77; blue). Despite the limited number of stations, a transition from the subpolar to subtropical gyre was clearly observed for NO_3^- concentration, $\delta^{15}N$, $\delta^{18}O$, and Δ(15–18) (i.e., NO_3^- $\delta^{15}N$—NO_3^- $\delta^{18}O$; Rafter et al., 2013) (Figure 3).

NO_3^- $\delta^{15}N$ and $\delta^{18}O$ were relatively homogenous at depths ≥1500 m (hereafter referred to as "deep ocean"; Figures 3b and 3c), with average values of 4.87‰ ± 0.13‰ and 1.98‰ ± 0.28‰ respectively, implying a Δ(15–18) of 2.89‰ ± 0.31‰ (Figure 3d). These deep ocean values are in good agreement with values reported for other North Atlantic sectors (Fawcett et al., 2015; Knapp et al., 2008; Marconi et al, 2015, 2019; Peng et al., 2018).

Table 1
Statistical Significance of Differences in NO_3^- $\delta^{15}N$ Values. (a) Average Values of NO_3^- $\delta^{15}N$ (‰), Sample Size (n) and Standard Deviation (SD) for Different Depth Ranges in the Four Studied Regions as Defined in Figure 1 and T-test Results Indicating Significance of the Difference Between the Means of Two Groups (P-values, P). (b) Comparison of the 600–1500 m Depth Range Between Stations South of the Subartic Front (SAF) With Main Basins North of the SAF and the Deep ocean

(a)

		NO_3^- $\delta^{15}N$ Average (‰)	n =	SD	South of SAF	Iceland basin	Irminger basin	Labrador basin	Deep ocean
South of SAF	150–600 m	4.41	19	0.14		$P < 0.001$	$P < 0.001$	$P < 0.001$	$P < 0.001$
	600–1500 m	4.65	21	0.17		$P < 0.001$	$P < 0.001$	$P < 0.001$	$P < 0.001$
	>1500 m	4.83	31	0.10		$P = 0.067$	$P = 0.079$	$P = 0.050$	$P = 0.080$
Iceland basin	150–600 m	4.90	17	0.14			$P = 0.600$	$P = 0.569$	$P = 0.438$
	600–1500 m	4.87	17	0.07			$P = 0.636$	$P = 0.791$	$P = 0.926$
	>1500 m	4.88	16	0.08			$P = 0.950$	$P = 0.948$	$P = 0.812$
Irminger basin	150–600 m	4.92	22	0.15				$P = 0.268$	$P = 0.104$
	600–1500 m	4.86	42	0.08				$P = 0.820$	$P = 0.523$
	>1500 m	4.88	23	0.11				$P = 0.899$	$P = 0.839$
Labrador basin	150–600 m	4.87	15	0.11					$P = 0.978$
	600–1500 m	4.86	19	0.07					$P = 0.770$
	>1500 m	4.88	24	0.10					$P = 0.728$
Deep ocean	All stations >1500 m	4.87	94	0.13					

(b)

South of SAF		NO_3^- $\delta^{15}N$ Average (‰)	n =	SD	St 17 & 21	Iceland basin	Irminger basin	Labrador basin	Deep ocean
St 1 & 13	600–1500 m	4.54	12	0.12	$P < 0.001$	$P < 0.001$	$P < 0.001$	$P < 0.001$	$P < 0.001$
St 17 & 21	600–1500 m	4.81	9	0.11		$P = 0.124$	$P = 0.182$	$P = 0.144$	$P = 0.198$

Stations located in the subpolar gyre (stations 26 to 77) presented relatively constant NO_3^- $\delta^{15}N$ values between 150 m depth and the seafloor, indistinguishable from the deep ocean signature (4.87‰ ± 0.13‰; p-value > 0.1), independent of the basin or depth range considered (Figure 3b; Table 1). NO_3^- $\delta^{15}N$ at stations south of the SAF (stations 1 to 21) was generally lower between 150 and 600 m depth (4.41‰ ± 0.14‰) compared to the deep ocean (p-value < 0.001; Table 1), reaching a NO_3^- $\delta^{15}N$ minimum around 300 m (ranging from 4.13‰ to 4.32‰). A relatively low NO_3^- $\delta^{15}N$ (4.65‰ ± 0.17‰) was also observed between 600 and 1500 m south of the SAF (p-value < 0.001; Table 1). However, this feature was mostly observed at stations 1 and 13 (4.54‰ ± 0.12‰, p-value < 0.001), with stations 17 and 21 presenting values close to the deep ocean signature (Table 1).

Despite a larger scatter apparent in the profiles, NO_3^- $\delta^{18}O$ did exhibit a different trend from the one of NO_3^- $\delta^{15}N$. NO_3^- $\delta^{18}O$ increased from the deep ocean (1.98‰ ± 0.28‰) to 150 m depth, associated with decreasing NO_3^- concentration (Figures 3a and 3c). This increase in NO_3^- $\delta^{18}O$ was largest for stations located south of the SAF, reaching up to 4.50‰ ± 0.28‰ at 150 m depth. The Irminger and Labrador basins presented the smallest increase in NO_3^- $\delta^{18}O$ toward the surface, reaching only 2.55‰ ± 0.17‰ at 150 m depth, while NO_3^- $\delta^{18}O$ increased to 3.27‰± 0.27‰ in the Iceland basin. This contrasting vertical evolution of NO_3^- $\delta^{15}N$ and $\delta^{18}O$ toward the surface led to deviations of Δ(15–18) relative to the deep ocean value (Figure 3d). For the stations located south of the SAF, the decrease in Δ(15–18) was driven by the combined increase in NO_3^- $\delta^{18}O$ and decrease in NO_3^- $\delta^{15}N$, while the decrease in Δ(15–18) for the stations in the subpolar gyre resulted from the increase in NO_3^- $\delta^{18}O$ only.

In the upper 150 m, both NO_3^- $\delta^{15}N$ and $\delta^{18}O$ increased up to 12.4‰ and 14.0‰ respectively (Figures 3b and 3c), while NO_3^- concentration decreased toward the surface (Figure 3a). Note that NO_3^- concentration was below the detection limit of the denitrifier method (<2 μmol l^{-1}) for most of the surface samples south of the SAF (i.e., upper 40 m at stations 1 to 21) and in the Labrador basin (i.e., upper 20 m at stations 69

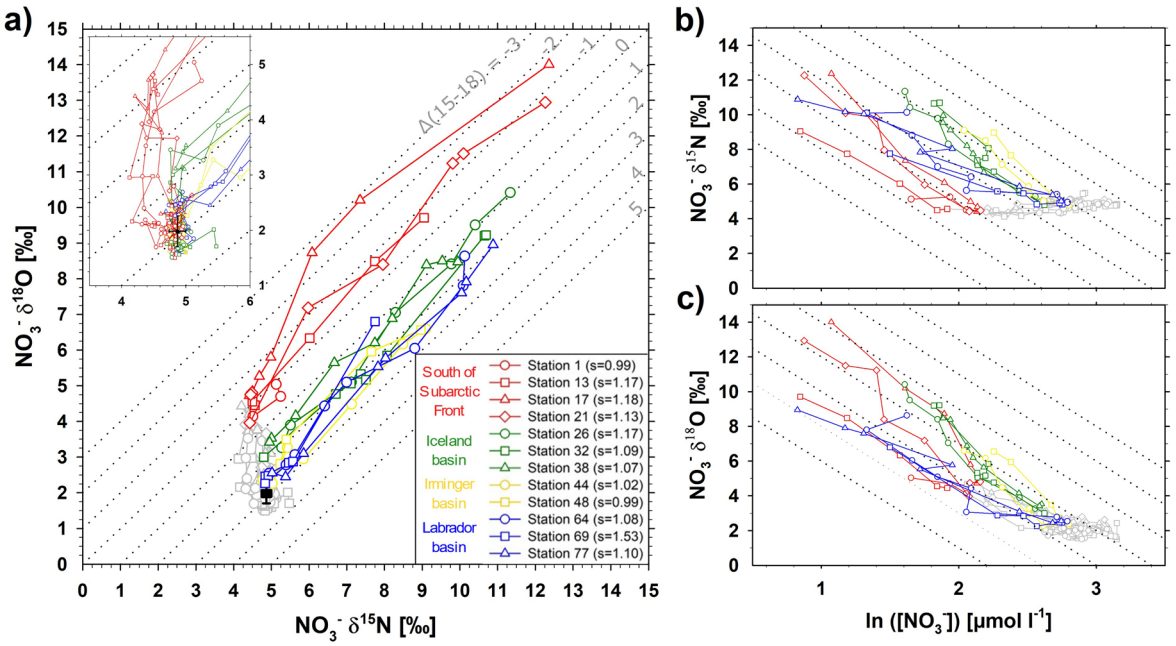

Figure 4. Plots of (a) NO_3^- $\delta^{18}O$ (‰) versus NO_3^- $\delta^{15}N$ (‰), (b) NO_3^- $\delta^{15}N$ (‰) versus ln([NO_3^-]) (µmol l^{-1}) and (c) NO_3^- $\delta^{18}O$ (‰) versus ln([NO_3^-]) (µmol l^{-1}) for all depth profiles (with colored data points for the upper 150 m, except in the insert of panel (a) where all data points are colored). Colors of GEOVIDE profiles refer to the four studied regions as in Figure 1: South of Subarctic Front (red), Iceland basin (green), Irminger basin (yellow) and Labrador basin (blue). In panel (a), the slope of the linear trendline for the upper 150 m is reported in the legend, the filled black square with error bars represents the average deep oceanic values (NO_3^- $\delta^{15}N$ = 4.87‰ ± 0.13‰ and NO_3^- $\delta^{18}O$ = 1.98‰ ± 0.28‰). Dotted black diagonal lines represent Δ(15–18) (‰) contours. In panels (b) and (c), dotted black diagonal lines represent fractionation trends with an isotope effect (ε) of 5‰.

and 77) (supporting information Table S1). Therefore, no surface nitrate isotope data are presented for these stations.

4. Discussion

4.1. Upper Ocean Nutrient Dynamics From the Subpolar to the Subtropical Gyre

4.1.1. Nitrate Assimilation and Ekman Transport in the Upper Ocean Layer

In the upper 150 m, the negative correlation between NO_3^- concentration and both NO_3^- $\delta^{15}N$ and $\delta^{18}O$ reflects the kinetic isotopic fractionation during NO_3^- assimilation (Figures 3a–3c). NO_3^- assimilation by phytoplankton preferentially incorporates ^{14}N into biomass, leaving the residual NO_3^- pool enriched in ^{15}N (Sigman et al., 1999; Wada & Hattori, 1978). This also holds for O isotopes, with the preferential conversion of ^{16}O compared to ^{18}O, but with the particularity that O atoms are not incorporated into biomass (i.e., NO_3^- being first converted to ammonium and then to organic N) (Granger et al., 2004, 2010; Karsh et al., 2012, 2014).

NO_3^- assimilation discriminates against the N and O isotopes to the same extent ($^{15}\varepsilon \sim {}^{18}\varepsilon$), as observed in laboratory culture experiments (Granger et al., 2010, 2004; Karsh et al., 2012) and field studies (DiFiore et al., 2009; Fawcett et al., 2015). Accordingly, in a NO_3^- $\delta^{18}O$ versus $\delta^{15}N$ space, residual NO_3^- falls along a line with a slope of 1, anchored on the isotopic composition of the initial NO_3^- pool (Sigman et al., 2005). Our observations clearly suggest that NO_3^- assimilation is the predominant driver of the NO_3^- isotopic composition in the upper 150 m along the entire transect (Figure 4a). We report slopes in the NO_3^- $\delta^{18}O$ versus $\delta^{15}N$ space ranging between 0.99 and 1.18 for the upper 150 m, indistinguishable from a slope of 1. The somewhat larger slope observed at station 69 in the Labrador basin (= 1.53) should be interpreted with care since this station has only one surface sample with high NO_3^- $\delta^{15}N$ and $\delta^{18}O$ values.

If NO_3^- assimilation proceeds with a constant isotope effect and if the reactant N pool (i.e., NO_3^-) is neither replenished nor subject to loss other than consumption, the isotopic evolutions of the residual NO_3^- pool

are described by Rayleigh fractionation kinetics, implying a linear relationship in a NO_3^- $\delta^{15}N$ or NO_3^- $\delta^{18}O$ versus ln($[NO_3^-]$) space and with the slope reflecting the negative isotope effect (Sigman et al., 1999). Negative linear correlations between NO_3^- $\delta^{15}N$ and ln($[NO_3^-]$), as well as between NO_3^- $\delta^{18}O$ and ln($[NO_3^-]$), further support assimilation of NO_3^- in the upper 150 m as the predominant process (Figures 4b and 4c). The isotope effects for stations located south of the SAF (stations 1, 13, 17, and 21) are 5.4‰ ± 0.6‰ ($R^2 = 0.82$, p-value < 0.001) and 6.1‰ ± 0.8‰ ($R^2 = 0.72$, p-value < 0.001) for NO_3^- $\delta^{15}N$ ($=^{15}\varepsilon$) and NO_3^- $\delta^{18}O$ ($=^{18}\varepsilon$), respectively. Stations in the Iceland basin (stations 26, 32, and 38) and Irminger basin (stations 44 and 48) present isotope effects of 5.9‰ ± 0.4‰ ($R^2 = 0.89$, p-value < 0.001) and 6.9‰ ± 0.4‰ ($R^2 = 0.92$, p-value < 0.001) for NO_3^- $\delta^{15}N$ and $\delta^{18}O$, respectively. These values fall within the range of isotope effects reported in the literature for other oceanic regions (Fripiat et al., 2019). In contrast, lower isotope effects are observed in the Labrador basin (stations 64, 6,9 and 77), with $^{15}\varepsilon$ and $^{18}\varepsilon$ being 3.3‰ ± 0.3‰ ($R^2 = 0.90$, p-value < 0.001) and 3.7‰ ± 0.3‰ ($R^2 = 0.90$, p-value < 0.001), respectively. These lower estimates are likely due to artifacts from mixing at these stations that are characterized by both NO_3^--depleted surface water and large vertical NO_3^- concentration gradients. Indeed, any resupply of NO_3^- to a water parcel that has experienced NO_3^- assimilation will deflect the isotopic signature of such water parcel downward from the Rayleigh fractionation line. The degree of deviation from the Rayleigh fractionation line increases with increasing degree of NO_3^- consumption (Sigman et al., 1999).

In the Irminger and Iceland basins (i.e., from subpolar gyre to SAF), a single relationship is observed between the degree of NO_3^- consumption and residual NO_3^- $\delta^{15}N$ and $\delta^{18}O$ (Figures 4b and 4c). This suggests that NO_3^- is supplied from a single source and progressively depleted by NO_3^- assimilation and export production. We suggest that NO_3^- is supplied by Ekman upwelling and deep winter convection, with Labrador Sea Water (LSW) as the ultimate source. NO_3^- is then progressively consumed during the Ekman transport of surface water from the subpolar gyre to the SAF. Just south of the SAF (stations 17 and 21), samples in the mixed layer fall on or slightly below the relationship observed in the Irminger and Iceland basins, while subsurface samples (i.e., below the mixed layer depth) clearly fall below it (Figures 4b and 4c). This suggests that assimilation of nitrate in the mixed layer at these stations (17 and 21) does not only draw on the local subsurface pool but more likely on the nitrate pool advected from the subpolar gyre. We thus argue that surface water just south of the SAF is also partly supplied in summer by Ekman transport across the inter-gyre boundary, in agreement with Oschlies (2002) and Williams and Follows (1998). Note that the deviation of the subsurface samples observed south of the SAF will be discussed in the following sections.

4.1.2. High Latitude Control on Low-Latitude Permanent Thermocline Properties

While NO_3^- assimilation controls the distribution of both NO_3^- concentration and its isotopic composition in the upper 150 m along the GEOVIDE transect, the characteristics of the subsurface NO_3^- pools (i.e., ~150 m depth) differ between basins. Indeed, the assimilation trends are parallel to each other in a NO_3^- $\delta^{18}O$ versus $\delta^{15}N$ space (Figure 4a), that is, starting from subsurface pools with different properties. While in the Labrador and Irminger basins the subsurface NO_3^- pool presents characteristics (i.e., $[NO_3^-]$, NO_3^- $\delta^{15}N$ and $\delta^{18}O$) close to the deep oceanic values, subsurface NO_3^- $\delta^{18}O$ progressively increases in the Iceland basin and in the subtropical gyre, uncorrelated to an increase in NO_3^- $\delta^{15}N$. In this section, we suggest that this decoupling of N and O isotopes in subsurface NO_3^- results from a combination of physical and biogeochemical processes that occur where the isopycnals representative of the low-latitude permanent thermocline (~27.4–27.5 kg m^{-3}) outcrop in the subpolar gyre. This imprint is then transmitted to the low-latitude permanent thermocline by isopycnal mixing (McCartney & Talley, 1982) and becomes progressively erased by low-latitude production and remineralization-nitrification processes (Sigman et al., 2009).

In the subpolar gyre, the occurrence of deep convection in winter (Clarke & Gascard, 1983; Pickart et al., 2003; Våge et al., 2008; Yashayaev, 2007) resets the upper 1500 m of the water column to the initial conditions (Holte et al., 2017; Yashayaev & Loder, 2016). This deep vertical mixing in winter implies that NO_3^- assimilation and remineralization-nitrification of sinking particles occur mostly within the same water parcel. The co-occurrence of NO_3^- assimilation and nitrification in the same water parcel has no effect on the NO_3^- N-isotope budget, as these processes are part of the internal cycle for N atoms. Indeed, remineralization of organic matter followed by nitrification produce NO_3^- with the same NO_3^- $\delta^{15}N$ as the assimilated NO_3^- (Marconi et al., 2019; Rafter et al., 2013; Sigman et al., 2005). In contrast, NO_3^- assimilation and nitrification are respectively a sink and a source for the O atoms. Their co-occurrence affects the

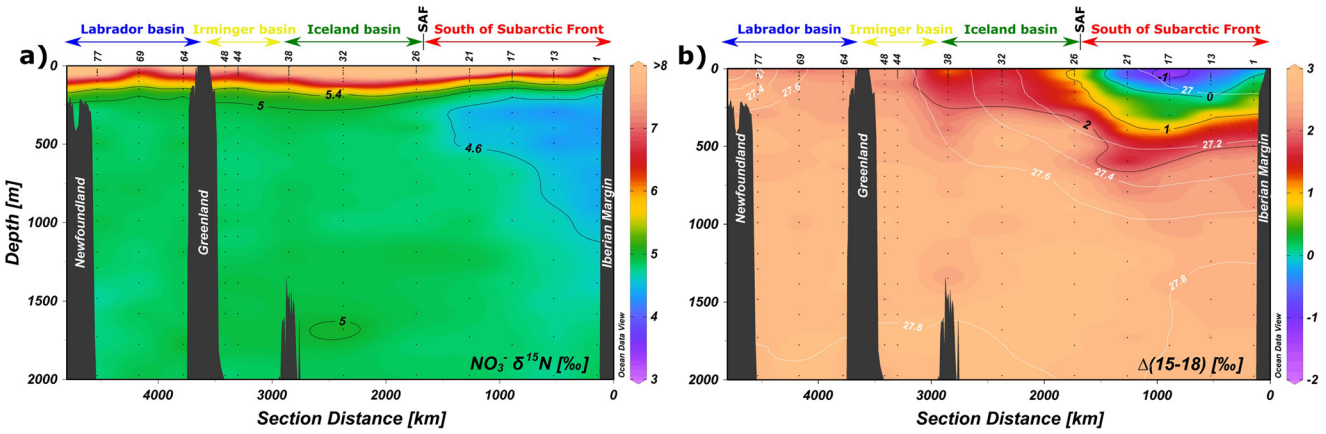

Figure 5. Vertical distribution of observed (a) NO_3^- $\delta^{15}N$ (‰) and (b) Δ(15–18) (‰) in the upper 2000 m. Colored arrows above the panels indicate the four studied regions as in Figure 1: South of Subarctic Front (red), Iceland basin (green), Irminger basin (yellow) and Labrador basin (blue). Overlaying white contours drawn in panel (b) represent winter potential density anomaly σ_0 at 0 dbar (kg m^{-3}) based on the World Ocean Database (WOA13; 1°; 1955–2012 January–March).

NO_3^- O-isotope budget (Fawcett et al., 2015; Sigman et al., 2009). Partial NO_3^- assimilation in the subpolar gyre causes NO_3^- $\delta^{18}O$ to increase since assimilated NO_3^- $\delta^{18}O$ is lower (down to −3‰) than NO_3^- produced by nitrification (i.e., H_2O $\delta^{18}O$ + 1.1‰; supporting information Figure S1) (Marconi et al., 2019; Peng et al., 2018). The co-occurrence of partial NO_3^- assimilation and nitrification in the same water parcel will, therefore, raise NO_3^- $\delta^{18}O$ while NO_3^- $\delta^{15}N$ remains constant, as observed (Figures 3c ,3d and 4a). This mechanism is likely more strongly expressed in the Iceland basin because of an overall higher export production (Falkowski et al., 1998) and lower prevailing NO_3^- concentration there.

South of the SAF, in the subtropical gyre, this increase in NO_3^- $\delta^{18}O$ is observed relatively deep in the water column (down to 600–800 m; Figure 3c), implying that this feature must be generated remotely. Indeed, the low-latitude permanent thermocline imposes a relatively shallow winter convection (<250 m) with most of the NO_3^- assimilation and nitrification occurring in the upper 250 m. This may partly explain the increase in NO_3^- $\delta^{18}O$ in the upper 250 m but not the increase deeper in the water column. We suggest that this deeper signal arises in the surface waters of the subpolar gyre before being transmitted to the low-latitude permanent thermocline by isopycnal mixing (McCartney & Talley, 1982). The comparison between Δ(15–18) and winter potential density anomaly contours further supports this hypothesis (Figure 5b), as Δ(15–18) values are similar along isopycnals.

In the subtropical gyre, the permanent thermocline waters recirculate from the eastern to the western North Atlantic (i.e., Sargasso Sea) following a predominant anticyclonic pattern. Nearly complete NO_3^- consumption in surface waters implies that assimilated NO_3^- is initially higher in NO_3^- $\delta^{18}O$ (2‰–4‰) than the regenerated NO_3^- $\delta^{18}O$ (H_2O $\delta^{18}O$ + 1.1‰; supporting information Figure S1; Marconi et al., 2019). A series of quantitative consumption-remineralization-nitrification cycles progressively decreases NO_3^- $\delta^{18}O$ toward regenerated NO_3^- $\delta^{18}O$ (Rafter et al., 2013; Sigman et al., 2009). This mechanism is in agreement with lower NO_3^- $\delta^{18}O$ values observed at equivalent isopycnals in the permanent thermocline of the Sargasso Sea (Fawcett et al., 2015).

4.2. N_2 Fixation and Influence of the Mediterranean Outflow

South of the SAF subsurface waters have lower NO_3^- $\delta^{15}N$ values than the deep ocean (Table 1; Figures 3c and 5a). Low NO_3^- $\delta^{15}N$ values are commonly reported in the subtropical gyre of the North Atlantic Ocean, a feature which has been mostly attributed to an incorporation of new N in surface waters by biological N_2 fixation (Bourbonnais et al., 2009; Fawcett et al., 2015; Knapp et al., 2008; Marconi et al., 2015, 2017, 2019; Riou et al., 2016). The $\delta^{15}N$ of organic N produced by N_2 fixation is estimated to range from −2‰ to 0‰ (Carpenter et al., 1997; Montoya et al., 2002). Remineralization of this low-$\delta^{15}N$ sinking particles, followed by nitrification, transmit this low-$\delta^{15}N$ signal to the subsurface NO_3^- pool (Bourbonnais et al., 2009; Knapp

et al., 2008). Alternatively, the low NO_3^- $\delta^{15}N$ may also result from the deposition of atmospheric N, harboring a $\delta^{15}N$ between −6‰ and −2‰ (Altieri et al., 2013; Hastings et al., 2003; Knapp et al., 2010). However, based on the work of Altieri et al. (2016) who show that N deposition primarily originates from a marine biogenic source, Marconi et al. (2019) estimated that atmospheric N deposition represents only 10% of the N_2 fixation inputs to the North Atlantic Ocean.

South of the SAF, N_2 fixation explains therefore both the low NO_3^- $\delta^{15}N$ values and a fraction of the decoupling between NO_3^- $\delta^{15}N$ and $\delta^{18}O$ (Figure 3). Here, lower subsurface Δ(15–18) values in comparison to the deep ocean are driven by the combined increase in NO_3^- $\delta^{18}O$ and a smaller decrease in NO_3^- $\delta^{15}N$ (Figure 3). While the increase in NO_3^- $\delta^{18}O$ likely results from the co-occurrence of partial NO_3^- assimilation and nitrification in the outcropping region of the permanent pycnocline (see Section 4.1.2), the decrease in NO_3^- $\delta^{15}N$ likely results from N_2 fixation in subtropical surface waters followed by remineralization-nitrification in the upper water column. Newly fixed N can be generated locally or remotely. Especially low-$\delta^{15}N$ NO_3^- is observed in subsurface waters in the western North Atlantic, as low as 2.5‰ (Fawcett et al., 2015; Knapp et al., 2008; Marconi et al., 2015; Van Oostende et al., 2017). The predominant anticyclonic circulation in the subtropical gyre will carry this low-$\delta^{15}N$ signal from the western North Atlantic to our studied area (Alvarez et al., 2002; Fernández-Castro et al., 2019). While an advection from the west is likely a significant contributor to the low subsurface NO_3^- $\delta^{15}N$, significant N_2 fixation rates (from 141 to 384.5 μmol N m^{-2} d^{-1}) were observed south of the SAF during GEOVIDE (stations 1 to 21) by Fonseca-Batista et al. (2019) using the $^{15}N_2$ dissolution incubation method (Großkopf et al., 2012; Mohr et al., 2010). These observations imply that the low NO_3^- $\delta^{15}N$ is partly generated locally. However, our data do not allow to differentiate the signal produced locally and the one advected from the west. Further investigations are needed to quantify their respective contribution to the low NO_3^- $\delta^{15}N$ observed in our studied area.

Close to the Iberian margin (stations 1 and 13), a low NO_3^- $\delta^{15}N$ signal is observed deep in the water column, that is, between 600 and 1500 m depth. Since most of the remineralization-nitrification of the sinking organic matter occurs above this depth, this signal must be generated remotely. Mediterranean Water (MW; Figure 1) is centered around 1000 m (i.e., salinity maximum in Figure 2b) and originates from the mixing of Mediterranean Outflow Water (MOW; ±34%) with subsurface (Eastern North Atlantic Central Water, ; ±57%) and intermediate waters (Labrador Surface Water and diluted Antarctic Intermediate Water; <10%) of the Northeast Atlantic basin (Carracedo et al., 2016). Low NO_3^- $\delta^{15}N$ is reported in the Mediterranean Sea, that is, 3.4‰ ± 0.5‰ for the western Mediterranean basin (Pantoja et al., 2002), and results from N_2 fixation (Pantoja et al., 2002) and/or atmospheric N deposition (Emeis et al., 2010; Mara et al., 2009). The co-occurrence of MW and low NO_3^- $\delta^{15}N$ in our studied area suggests that the Mediterranean Sea has an impact on NO_3^- $\delta^{15}N$ in the North Atlantic Ocean.

To assess the influence of MW on NO_3^- $\delta^{15}N$ profiles along the transect, we used an isotopic mixing model coupled with the results of an extended Optimum Multi-Parameter (eOMP) analysis performed for the GEOVIDE cruise, which returns the mixing proportions of different source water types (García-Ibáñez et al., 2018). First, we built a "flat" NO_3^- $\delta^{15}N$ profile by setting the NO_3^- $\delta^{15}N$ of all the water masses to the average deep ocean value (4.82‰ ± 0.05‰) reported by Marconi et al. (2019). The latter is indistinguishable from the values reported in the present study (4.87‰ ± 0.13‰). This approach is predicated on the idea that NO_3^- is supplied via Ekman upwelling and deep winter convection over the entire subpolar gyre, yielding subsurface waters with NO_3^- isotopic composition indistinguishable from deep ocean values, which is subsequently transmitted south of the SAF by isopycnal mixing (see discussions above). To extract the contribution of MOW to the MW, we used the results of a different eOMP performed by Carracedo et al. (2016) who solved the mixing near Cape St. Vincente (Portugal) between the Mediterranean Outflow Water (MOW; with NO_3^- $\delta^{15}N$ being set at 3.5‰ ± 0.5‰, Pantoja et al., 2002) and other source waters since the point of overflow from the Mediterranean basin (being set to the deep ocean $\delta^{15}N$ value for this analysis). Our isotopic mixing model based on the eOMP performed by Carracedo et al. (2016) shows that the signature of MW NO_3^- $\delta^{15}N$ is 4.42‰ ± 0.13‰. Using this MW signature and the eOMP performed by García-Ibáñez et al. (2018), the resulting NO_3^- $\delta^{15}N$ profiles returned by our isotopic mixing model (i.e., thick purple lines in Figure 6) at the selected stations (based on their proximity to the Iberian Peninsula) reveal that an advection of the Mediterranean signal is indeed able to reproduce the low NO_3^- $\delta^{15}N$ values observed between 600 and 1500 m depth south of the SAF (i.e., red profiles in Figure 6). As the proportion of MW decreases with

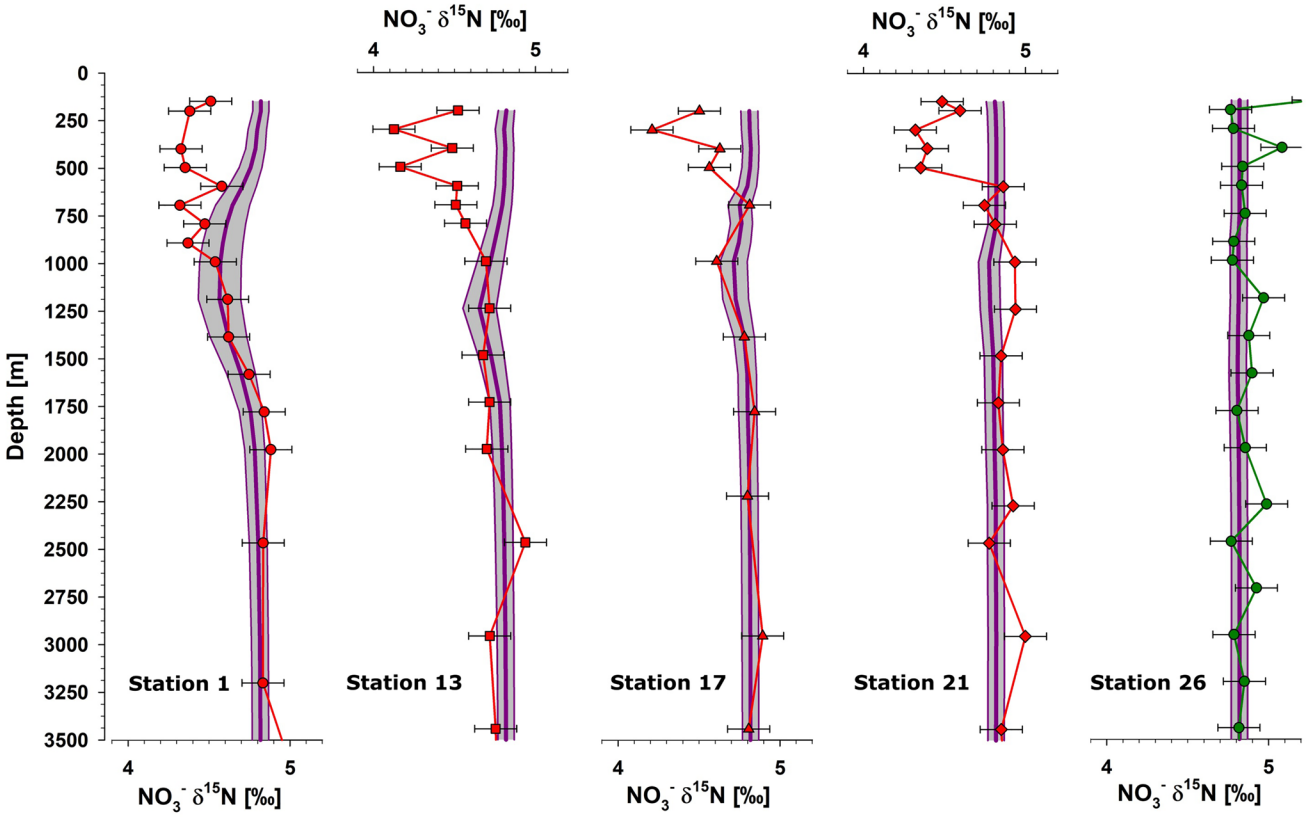

Figure 6. Observed NO_3^- $\delta^{15}N$ (‰) profiles (symbols and colors as in Figure 3) and modeled NO_3^- $\delta^{15}N$ (‰) profiles (thick purple lines) generated using an isotopic mixing model coupled with the results of an extended Optimum Multi-Parameters (eOMP) analysis to study the influence of the Mediterranean Water (see text for details) along the eastern part of the GEOTRACES GA01 (GEOVIDE) transect with increasing distance from the Iberian margin (from station 1 to station 26). Error bars for measured profiles correspond to 1 SD (=0.13‰), while error for the model outputs is shown by the gray shaded envelop (see text for details).

increasing distance from the Iberian margin (García-Ibáñez et al., 2018; see also Figure 2b), its influence on NO_3^- isotopic composition decreases, in agreement with our modeled values and observations from station 1 to station 26. Note that the influence of MW on NO_3^- $\delta^{15}N$ could not be traced anymore north of the SAF (i.e., station 26 in Figure 6).

However, the advection of the MW signal is unable to fully account for the NO_3^- $\delta^{15}N$ minimum observed between 150 and 600 m depth south of the SAF (stations 1 to 21), where the Eastern North Atlantic Central Water (ENACW) is the dominant water mass (>50%; $27.0 < \sigma_0 < 27.3$; García-Ibáñez et al., 2018). Therefore, the low NO_3^- $\delta^{15}N$ observed in ENACW is likely the result of both local N_2 fixation and a signal advected from the western North Atlantic, as discussed above. In the present study, the NO_3^- $\delta^{15}N$ value of samples for which ENACW > 50% (n = 19) averaged 4.41‰ ± 0.14‰ while NO_3^- concentration averaged 9.9 ± 1.6 μmol l^{-1}. These values fall within the range reported by Marconi et al. (2019) for NACW (>20°N) (with NO_3^- $\delta^{15}N$ = 4.40 ‰± 1.80‰, ranging from 2.67‰ to 16.45‰, and NO_3^- concentration = 9.17 ± 4.88 μmol l^{-1}). The wider range reported by Marconi et al. (2019) likely results from the inclusion of surface samples impacted by nitrate assimilation and from other types of NACW encountered. Note that, while the proportion of ENACW rapidly decreases (<50%) north of the SAF, no NO_3^- $\delta^{15}N$ minimum is observed in subsurface waters (see station 26 in Figure 6).

To conclude, our study shows that not only is N_2 fixation important to generate the pool of low NO_3^- $\delta^{15}N$ in the North Atlantic Ocean, but that an influence from the Mediterranean Sea needs to be also considered to solve the NO_3^- isotopic budget in the eastern North Atlantic Ocean.

4.3. Paleoceanographic Implications

The North Atlantic Ocean is a key component of the meridional overturning circulation and climate in general (Broecker, 1998; Denton et al., 2010; Talley, 2013). The isotopic ratio of N preserved in sedimentary records of the North Atlantic Ocean is a promising tool to reconstruct either surface nitrate concentration in the past, thereby providing insights into past circulation in the high-latitude Atlantic Ocean (Straub, Trembly, et al., 2013), or variations in the intensity of N_2 fixation (Straub, Sigman, et al., 2013). The strong relationship between the degree of NO_3^- consumption and residual NO_3^- $\delta^{15}N$ from the subpolar gyre to the SAF (Figure 4b) supports the usefulness of sedimentary N $\delta^{15}N$ to reconstruct past degree of NO_3^- consumption and thus surface NO_3^- concentration. However, south of the SAF, complete NO_3^- consumption requires that sinking organic N $\delta^{15}N$ is similar to the supplied NO_3^- $\delta^{15}N$. Our study shows that the regional subsurface NO_3^- $\delta^{15}N$ supplying surface waters is depleted in ^{15}N due to N_2 fixation (Figure 5a). Therefore, a shift in the location of the SAF needs to be considered when interpreting sedimentary $\delta^{15}N$ records of the North Atlantic Ocean, as the driver for the sedimentary $\delta^{15}N$ signal will not be the same north and south of the SAF.

5. Conclusion

The NO_3^- isotopic composition along the GEOTRACES GA01 transect reveals the impact of high-latitude processes on low-latitude areas of the North Atlantic Ocean, with a southward supply of NO_3^- occurring both in the surface waters by wind-driven Ekman transport and in the permanent thermocline via isopycnal mixing. While the co-occurrence of partial assimilation and nitrification at high-latitudes leads to high NO_3^- $\delta^{18}O$ values, this elevated signal is progressively erased during the recirculation in the subtropical gyre due to the increasing influence of regenerated NO_3^- $\delta^{18}O$ imprint. In addition, our study shows the impact of N_2 fixation on NO_3^- isotopic composition in the temperate Northeast Atlantic Ocean as well as the influence of the Mediterranean outflow deeper in the water column, suggesting that the latter needs to be taken into account to solve the NO_3^- isotopic budget in the eastern North Atlantic Ocean.

Data Availability Statement

Data are available in supporting information Table S1 and from the LEFE-CYBER database at the address: http://www.obs-vlfr.fr/proof/ftpfree/geovide/db/DATA/NITRATE_ISOTOPY/.

Acknowledgments
The authors thank the captain and crew of the R/V *Pourquoi Pas?* for organizing the logistics on board as well as chief scientists G. Sarthou and P. Lherminier for their assistance and support during the GEOVIDE expedition. P. Lherminier, P. Tréguer, F. Pérez and C. Schmechtig are acknowledged for providing CTD and nutrients concentration data. The GEOVIDE project was co-funded by the French national program LEFE/INSU (GEOVIDE), ANR Blanc (GEOVIDE) and RPDOC, LabEX MER and IFREMER. F. Deman was supported by the Belgian Federal Science Policy Office (Belspo contract BL/12/C63) while writing the manuscript. This work was financed by Flanders Research Foundation (FWO contract G0715.12N) and Vrije Universiteit Brussel, R&D, Strategic Research Plan "Tracers of Past & Present Global Changes". During the preparation of the manuscript, Debany Fonseca-Batista was supported by funding from the Canada First Research Excellence Fund, through an International Postdoctoral Fellowship of the Ocean Frontier Institute (OFI) at Dalhousie University.

References

Altieri, K. E., Fawcett, S. E., Peters, A. J., Sigman, D. M., & Hastings, M. G. (2016). Marine biogenic source of atmospheric organic nitrogen in the subtropical North Atlantic. *Proceedings of the National Academy of Sciences of the United States of America*, *113*(4), 925–930. https://doi.org/10.1073/pnas.1516847113

Altieri, K. E., Hastings, M. G., Gobel, A. R., Peters, A. J., & Sigman, D. M. (2013). Isotopic composition of rainwater nitrate at Bermuda: The influence of air mass source and chemistry in the marine boundary layer. *Journal of Geophysical Research Atmospheres*, *118*(19), 11304–11316. https://doi.org/10.1002/jgrd.50829

Álvarez, M., Bryden, H. L., Pérez, F. F., Ríos, A. F., & Rosón, G. (2002). Physical and biogeochemical fluxes and net budgets in the subpolar and temperate North Atlantic. *Journal of Marine Research*, *60*(2), 191–226. https://doi.org/10.1357/00222400260497462

Bigg, G. R., & Rohling, E. J. (2000). An oxygen isotope data set for marine waters. *Journal of Geophysical Research*, *105*(C4), 8527–8535. https://doi.org/10.1029/2000jc900005

Böhlke, J. K., Mroczkowski, S. J., & Coplen, T. B. (2003). Oxygen isotopes in nitrate: New reference materials for 18O:17O:16O measurements and observations on nitrate-water equilibration. *Rapid Communications in Mass Spectrometry*, *17*, 1835–1846. https://doi.org/10.1002/rcm.1123

Bourbonnais, A., Lehmann, M. F., Waniek, J. J., & Schulz-Bull, D. E. (2009). Nitrate isotope anomalies reflect N_2 fixation in the Azores Front region (subtropical NE Atlantic). *Journal of Geophysical Research*, *114*(3), 1–16. https://doi.org/10.1029/2007jc004617

Broecker, W. S. (1998). Paleocean circulation during the last deglaciation: A bipolar seesaw? *Paleoceanography*, *13*(2), 119–121. https://doi.org/10.1029/97pa03707

Buckley, M. W., & Marshall, J. (2016). Observations, inferences, and mechanisms of the Atlantic Meridional Overturning Circulation: A review. *Reviews of Geophysics*, *54*, 5–63. https://doi.org/10.1002/2015rg000493

Capone, D. G., Bronk, D. A., Mulholland, M. R., & Carpenter, E. J. (2008). *Nitrogen in the marine environment*. Elsevier. https://doi.org/10.1016/B978-0-12-372522-6.X0001-1

Capone, D. G., Burns, J. A., Montoya, J. P., Subramaniam, A., Mahaffey, C., Gunderson, T., et al. (2005). Nitrogen fixation by *Trichodesmium* spp: An important source of new nitrogen to the tropical and subtropical North Atlantic Ocean. *Global Biogeochemical Cycles*, *19*(2), 1–17. https://doi.org/10.1029/2004gb002331

Carpenter, E. J., Harvey, H. R., Fry, B., & Capone, D. G. (1997). Biogeochemical tracers of the marine cyanobacterium *Trichodesmium*. *Deep Sea Research: Oceanographic Research Papers*, *44*(1), 27–38. https://doi.org/10.1016/s0967-0637(96)00091-x

Carracedo, L. I., Pardo, P. C., Flecha, S., & Pérez, F. F. (2016). On the Mediterranean water composition. *Journal of Physical Oceanography*, *46*(4), 1339–1358. https://doi.org/10.1175/jpo-d-15-0095.1

Casciotti, K. L., Sigman, D. M., Hastings, M. G., Böhlke, J. K., & Hilkert, A. (2002). Measurement of the oxygen isotopic composition of nitrate in seawater and freshwater using the denitrifier method. *Analytical Chemistry*, *74*(19), 4905–4912. https://doi.org/10.1021/ac020113w

Clarke, R. A., & Gascard, J.-C. (1983). The formation of Labrador Sea water. Part I: Large-scale processes. *Journal of Physical Oceanography*, *13*, 1764–1778. https://doi.org/10.1175/1520-0485(1983)013<1764:tfolsw>2.0.co;2

Daniault, N., Mercier, H., Lherminier, P., Sarafanov, A., Falina, A., Zunino, P., et al. (2016). The northern North Atlantic Ocean mean circulation in the early 21st century. *Progress in Oceanography*, *146*, 142–158. https://doi.org/10.1016/j.pocean.2016.06.007

Denton, G. H., Anderson, R. F., Toggweiler, J. R., Edwards, R. L., Schaefer, J. M., & Putnam, A. E. (2010). The last glacial termination. *Science*, *328*(5986), 1652–1656. https://doi.org/10.1126/science.1184119

Deutsch, C., Sarmiento, J. L., Sigman, D. M., Gruber, N., & Dunne, J. P. (2007). Spatial coupling of nitrogen inputs and losses in the ocean. *Nature*, *445*(7124), 163–167. https://doi.org/10.1038/nature05392

DeVries, T., Deutsch, C., Rafter, P. A., & Primeau, F. (2013). Marine denitrification rates determined from a global 3-D inverse model. *Biogeosciences*, *10*(4), 2481–2496. https://doi.org/10.5194/bg-10-2481-2013

DiFiore, P. J., Sigman, D. M., & Dunbar, R. B. (2009). Upper ocean nitrogen fluxes in the Polar Antarctic Zone: Constraints from the nitrogen and oxygen isotopes of nitrate. *Geochemistry, Geophysics, Geosystems*, *10*(11), Q11016. https://doi.org/10.1029/2009gc002468

Emeis, K. C., Mara, P., Schlarbaum, T., Möbius, J., Dähnke, K., Struck, U., et al. (2010). External N inputs and internal N cycling traced by isotope ratios of nitrate, dissolved reduced nitrogen, and particulate nitrogen in the eastern Mediterranean Sea. *Journal of Geophysical Research*, *115*(4), 1–16. https://doi.org/10.1029/2009jg001214

Falkowski, P. G., Barber, R. T., & Smetacek, V. (1998). Biogeochemical controls and feedbacks on ocean primary production. *Science*, *281*(5374), 200–206. https://doi.org/10.1126/science.281.5374.200

Fawcett, S. E., Ward, B. B., Lomas, M. W., & Sigman, D. M. (2015). Vertical decoupling of nitrate assimilation and nitrification in the Sargasso Sea. *Deep Sea Research Part I: Oceanographic Research Papers*, *103*, 64–72. https://doi.org/10.1016/j.dsr.2015.05.004

Fernández-Castro, B., Álvarez, M., Nieto-Cid, M., Zunino, P., Mercier, H., & Álvarez-Salgado, X. A. (2019). Dissolved organic nitrogen production and export by meridional overturning in the eastern subpolar North Atlantic. *Geophysical Research Letters*, *46*(7), 3832–3842. https://doi.org/10.1029/2018GL080284

Follows, M., & Dutkiewicz, S. (2002). Meteorological modulation of the North Atlantic spring bloom. *Deep-Sea Research Part II: Topical Studies in Oceanography*, *49*(1–3), 321–344. https://doi.org/10.1016/S0967-0645(01)00105-9

Fonseca-Batista, D., Li, X., Riou, V., Michotey, V., Deman, F., Fripiat, F., et al. (2019). Evidence of high N_2 fixation rates in the temperate northeast Atlantic. *Biogeosciences*, *16*(5), 999–1017. https://doi.org/10.5194/bg-16-999-2019

Fripiat, F., Martínez-García, A., Fawcett, S. E., Kemeny, P. C., Studer, A. S., Smart, S. M., et al. (2019). The isotope effect of nitrate assimilation in the Antarctic Zone: Improved estimates and paleoceanographic implications. *Geochimica et Cosmochimica Acta*, *247*, 261–279. https://doi.org/10.1016/j.gca.2018.12.003

García-Ibáñez, M. I., Pérez, F. F., Lherminier, P., Zunino, P., Mercier, H., & Tréguer, P. (2018). Water mass distributions and transports for the 2014 GEOVIDE cruise in the North Atlantic. *Biogeosciences*, *15*(7), 2075–2090. https://doi.org/10.5194/bg-15-2075-201

Gonfiantini, R., Stichler, W., & Rozanski, K. (1995). Standards and intercomparison materials distributed by the international atomic energy agency for stable isotope measurements. In *Proceedings of a consultants meeting held in Vienna, 1–3 December 1993* (p. 13–29). IAEA. https://doi.org/10.1016/0375-6505(95)00024-0

Granger, J., & Sigman, D. M. (2009). Removal of nitrite with sulfamic acid for nitrate N and O isotope analysis with the denitrifier method. *Rapid Communications in Mass Spectrometry*, *23*(23), 3753–3762. https://doi.org/10.1002/rcm.4307

Granger, J., Sigman, D. M., Needoba, J. A., & Harrison, P. J. (2004). Coupled nitrogen and oxygen isotope fractionation of nitrate during assimilation by cultures of marine phytoplankton. *Limnology and Oceanography*, *49*(5), 1763–1773. https://doi.org/10.4319/lo.2004.49.5.1763

Granger, J., Sigman, D. M., Rohde, M. M., Maldonado, M. T., & Tortell, P. D. (2010). N and O isotope effects during nitrate assimilation by unicellular prokaryotic and eukaryotic plankton cultures. *Geochimica et Cosmochimica Acta*, *74*(3), 1030–1040. https://doi.org/10.1016/j.gca.2009.10.044

Grasshoff, K., Krembling, K., & Ehrhardt, M. (1999). *Methods of seawater analysis*. Wiley-VCH.

Großkopf, T., Mohr, W., Baustian, T., Schunck, H., Gill, D., Kuypers, M. M. M., et al. (2012). Doubling of marine dinitrogen-fixation rates based on direct measurements. *Nature*, *488*(7411), 361–364. https://doi.org/10.1038/nature11338

Gruber, N., & Galloway, J. N. (2008). An Earth-system perspective of the global nitrogen cycle. *Nature*, *451*(7176), 293–296. https://doi.org/10.1038/nature06592

Harrison, G. W., Yngve Børsheim, K., Li, W. K. W., Maillet, G. L., Pepin, P., Sakshaug, E., et al. (2013). Phytoplankton production and growth regulation in the Subarctic North Atlantic: A comparative study of the Labrador Sea-Labrador/Newfoundland shelves and Barents/Norwegian/Greenland seas and shelves. *Progress in Oceanography*, *114*, 26–45. https://doi.org/10.1016/j.pocean.2013.05.003

Hastings, M. G., Sigman, D. M., & Lipschultz, F. (2003). Isotopic evidence for source changes of nitrate in rain at Bermuda. *Journal of Geophysical Research*, *108*(D24). 4790. https://doi.org/10.1029/2003jd003789

Henson, S. A., Dunne, J. P., & Sarmiento, J. L. (2009). Decadal variability in North Atlantic phytoplankton blooms. *Journal of Geophysical Research*, *114*(4), 1–11. https://doi.org/10.1029/2008jc005139

Holte, J., Talley, L. D., Gilson, J., & Roemmich, D. (2017). An Argo mixed layer climatology and database. *Geophysical Research Letters*, *44*(11), 5618–5626. https://doi.org/10.1002/2017gl073426. https://doi.org/10.1002/2017GL073426

Karsh, K. L., Granger, J., Kritee, K., & Sigman, D. M. (2012). Eukaryotic assimilatory nitrate reductase fractionates N and O isotopes with a ratio near unity. *Environmental Science & Technology*, *46*(11), 5727–5735. https://doi.org/10.1021/es204593q

Karsh, K. L., Trull, T. W., Sigman, D. M., Thompson, P. A., & Granger, J. (2014). The contributions of nitrate uptake and efflux to isotope fractionation during algal nitrate assimilation. *Geochimica et Cosmochimica Acta*, *132*, 391–412. https://doi.org/10.1016/j.gca.2013.09.030

Knapp, A. N., DiFiore, P. J., Deutsch, C., Sigman, D. M., & Lipschultz, F. (2008). Nitrate isotopic composition between Bermuda and Puerto Rico: Implications for N_2 fixation in the Atlantic Ocean. *Global Biogeochemical Cycles*, *22*, 1–14. https://doi.org/10.1029/2007gb003107

Knapp, A. N., Hastings, M. G., Sigman, D. M., Lipschultz, F., & Galloway, J. N. (2010). The flux and isotopic composition of reduced and total nitrogen in Bermuda rain. *Marine Chemistry*, *120*(1–4), 83–89. https://doi.org/10.1016/j.marchem.2008.08.007

Lherminier, P., & Sarthou, G. (2017). *The 2014 Greenland-Portugal GEOVIDE CTDO2 hydrographic and SADCP data (GO-SHIP A25 and GEOTRACES GA01)*. SEANOE. https://doi.org/10.17882/52153

Longhurst, A. (2007). *Ecological geography of the sea*. Elsevier.

Mara, P., Mihalopoulos, N., Gogou, A., Daehnke, K., Schlarbaum, T., Emeis, K. C., & Krom, M. (2009). Isotopic composition of nitrate in wet and dry atmospheric deposition on Crete in the eastern Mediterranean Sea GB4002. *Global Biogeochemical Cycles*, *23*(4), 1–11. https://doi.org/10.1029/2008gb003395

Marconi, D., Alexandra Weigand, M., Rafter, P. A., McIlvin, M. R., Forbes, M., Casciotti, K. L., & Sigman, D. M. (2015). Nitrate isotope distributions on the US GEOTRACES North Atlantic cross-basin section: Signals of polar nitrate sources and low latitude nitrogen cycling. *Marine Chemistry*, *177*, 143–156. https://doi.org/10.1016/j.marchem.2015.06.007

Marconi, D., Sigman, D. M., Casciotti, K. L., Campbell, E. C., Alexandra Weigand, M., Fawcett, S. E., et al. (2017). Tropical Dominance of N_2 Fixation in the North Atlantic Ocean. *Global Biogeochemical Cycles*, *31*(10), 1608–1623. https://doi.org/10.1002/2016gb005613

Marconi, D., Weigand, M. A., & Sigman, D. M. (2019). Nitrate isotopic gradients in the North Atlantic Ocean and the nitrogen isotopic composition of sinking organic matter. *Deep Sea Research Part I: Oceanographic Research Papers*, *145*, 109–124. https://doi.org/10.1016/j.dsr.2019.01.010

Martin, P., Lampitt, R. S., Jane Perry, M., Sanders, R., Lee, C., & D'Asaro, E. (2011). Export and mesopelagic particle flux during a North Atlantic spring diatom bloom. *Deep Sea Research Part I: Oceanographic Research Papers*, *58*(4), 338–349. https://doi.org/10.1016/j.dsr.2011.01.006

McCartney, M. S., & Talley, L. D. (1982). The subpolar mode water of the North Atlantic Ocean. *Journal of Physical Oceanography*, *12*, 1169–1188. https://doi.org/10.1175/1520-0485(1982)012<1169:TSMWOT>2.0.CO;2

Mohr, W., Großkopf, T., Wallace, D. W. R., & LaRoche, J. (2010). Methodological underestimation of oceanic nitrogen fixation rates. *PLOS ONE*, *5*(9), 1–7. https://doi.org/10.1371/journal.pone.0012583

Montoya, J. P., Carpenter, E. J., & Capone, D. G. (2002). Nitrogen fixation and nitrogen isotope abundances in zooplankton of the oligotrophic North Atlantic. *Limnology and Oceanography*, *47*(6), 1617–1628. https://doi.org/10.4319/lo.2002.47.6.1617

Moore, C. M., Mills, M. M., Arrigo, K. R., Berman-Frank, I., Bopp, L., Boyd, P. W., et al. (2013). Processes and patterns of oceanic nutrient limitation. *Nature Geoscience*, *6*(9), 701–710. https://doi.org/10.1038/ngeo1765

Moore, C. M., Mills, M. M., Langlois, R., Milne, A., Achterberg, E. P., La Roche, J., & Geider, R. J. (2008). Relative influence of nitrogen and phosphorous availability on phytoplankton physiology and productivity in the oligotrophic sub-tropical North Atlantic Ocean. *Limnology and Oceanography*, *53*(1), 291–305. https://doi.org/10.4319/lo.2008.53.1.0291

Oschlies, A. (2002). Nutrient supply to the surface waters of the North Atlantic: A model study. *Journal of Geophysical Research*, *107*(C5), 3046. https://doi.org/10.1029/2000jc000275

Pantoja, S., Repeta, D. J., Sachs, J. P., & Sigman, D. M. (2002). Stable isotope constraints on the nitrogen cycle of the Mediterranean Sea water column. *Deep-Sea Research*, *49*(9), 1909–1621. https://doi.org/10.1016/s0967-0637(02)00066-3

Peng, X., Fawcett, S. E., Van Oostende, N., Wolf, M. J., Marconi, D., Sigman, D. M., & Ward, B. B. (2018). Nitrogen uptake and nitrification in the subarctic North Atlantic Ocean. *Limnology and Oceanography*, *63*, 1462–1487. https://doi.org/10.1002/lno.10784

Perez, F. F., Treguer, P., Branellec, P., García-Ibáñez, M. I., Lherminier, P., & Sarthou, G. (2018). *The 2014 Greenland-Portugal GEOVIDE bottle data (GO-SHIP A25 and GEOTRACES GA01)*. SEANOE. https://doi.org/10.17882/54653

Pickart, R. S., Spall, M. A., Ribergaard, M. H., Moore, G. W. K., & Milliff, R. F. (2003). Deep convection in the Irminger Sea forced by the Greenland tip jet. *Nature*, *424*(6945), 152–156. https://doi.org/10.1038/nature01729

Rafter, P. A., Difiore, P. J., & Sigman, D. M. (2013). Coupled nitrate nitrogen and oxygen isotopes and organic matter remineralization in the Southern and Pacific Oceans. *Journal of Geophysical Research: Oceans*, *118*(10), 4781–4794. https://doi.org/10.1002/jgrc.20316

Riou, V., Fonseca-Batista, D., Roukaerts, A., Biegala, I. C., Prakya, S. R., Loureiro, C. M., et al. (2016). Importance of N_2-fixation on the productivity at the north-western Azores current/front system, and the abundance of diazotrophic unicellular cyanobacteria. *PLOS ONE*, *11*(3), 1–22. https://doi.org/10.1371/journal.pone.0150827

Rossby, T. (1996). The North Atlantic Current and surrounding waters: At the crossroads. *Reviews of Geophysics*, *34*(4), 463–481. https://doi.org/10.1029/96rg02214

Sanders, R., Henson, S. A., Koski, M., De La Rocha, C. L., Painter, S. C., Poulton, A. J., et al. (2014). The biological carbon pump in the North Atlantic. *Progress in Oceanography*, *129*(PB), 200–218. https://doi.org/10.1016/j.pocean.2014.05.005

Sarthou, G., Lherminier, P., Achterberg, E. P., Alonso-Pérez, F., Bucciarelli, E., Boutorh, J., & Zunino, P. (2018). Introduction to the French GEOTRACES North Atlantic transect (GA01): GEOVIDE cruise. *Biogeosciences*, *15*(23), 7097–7109. https://doi.org/10.5194/bg-15-7097-2018

Sigman, D. M., Altabet, M. A., McCorkle, D. C., Francois, R., & Fischer, G. (1999). The δ15N of nitrate in the Southern Ocean: Consumption of nitrate in surface waters. *Global Biogeochemical Cycles*, *13*(4), 1149–1166. https://doi.org/10.1029/1999gb900038

Sigman, D. M., Casciotti, K. L., Andreani, M., Barford, C., Galanter, M., & Böhlke, J. K. (2001). A bacterial method for the nitrogen isotopic analysis of nitrate in seawater and freshwater. *Analytical Chemistry*, *73*(17), 4145–4153. https://doi.org/10.1021/ac010088e

Sigman, D. M., DiFiore, P. J., Hain, M. P., Deutsch, C., Wang, Y., Karl, D. M., et al. (2009). The dual isotopes of deep nitrate as a constraint on the cycle and budget of oceanic fixed nitrogen. *Deep Sea Research Part I: Oceanographic Research Papers*, *56*(9), 1419–1439. https://doi.org/10.1016/j.dsr.2009.04.007

Sigman, D. M., Granger, J., DiFiore, P. J., Lehmann, M. M., Ho, R., Cane, G., & van Geen, A. (2005). Coupled nitrogen and oxygen isotope measurements of nitrate along the eastern North Pacific margin. *Global Biogeochemical Cycles*, *19*(4), 1–14. https://doi.org/10.1029/2005gb002458

Straub, M., Sigman, D. M., Ren, H., Martínez-García, A., Meckler, A. N., Hain, M. P., & Haug, G. H. (2013). Changes in North Atlantic nitrogen fixation controlled by ocean circulation. *Nature*, *501*(7466), 200–203. https://doi.org/10.1038/nature12397

Straub, M., Tremblay, M. M., Sigman, D. M., Studer, A. S., Ren, H., Toggweiler, J. R., & Haug, G. H. (2013). Nutrient conditions in the subpolar North Atlantic during the last glacial period reconstructed from foraminifera-bound nitrogen isotopes. *Paleoceanography*, *28*(1), 79–90. https://doi.org/10.1002/palo.20013

Talley, L. (2013). Closure of the global overturning circulation through the Indian, Pacific, and Southern oceans: Schematics and transports. *Oceanography*, *26*(1), 80–97. https://doi.org/10.5670/oceanog.2013.07

Våge, K., Pickart, R. S., Thierry, V., Reverdin, G., Lee, C. M., Petrie, B., et al. (2008). Surprising return of deep convection to the subpolar North Atlantic Ocean in winter 2007–2008. *Nature Geoscience*, *2*(1), 67–72. https://doi.org/10.1038/ngeo382

Van Oostende, N., Fawcett, S. E., Marconi, D., Lueders-Dumont, J., Sabadel, A. J. M., Woodward, E. M. S., et al. (2017). Variation of summer phytoplankton community composition and its relationship to nitrate and regenerated nitrogen assimilation across the North Atlantic Ocean. *Deep Sea Research Part I: Oceanographic Research Papers*, *12*, 79–94. https://doi.org/10.1016/j.dsr.2016.12.012

Wada, E., & Hattori, A. (1978). Nitrogen isotope effects in the assimilation of inorganic nitrogenous compounds by marine diatoms. *Geomicrobiology Journal*, *1*(1), 85–101. https://doi.org/10.1080/01490457809377725

Weigand, M. A., Foriel, J., Barnett, B., Oleynik, S., & Sigman, D. M. (2016). Updates to instrumentation and protocols for isotopic analysis of nitrate by the denitrifier method. *Rapid Communications in Mass Spectrometry*, *30*, 1365–1383. https://doi.org/10.1002/rcm.7570

Williams, R. G., & Follows, M. J. (1998). The Ekman transfer of nutrients and maintenance of new production over the North Atlantic. *Deep Sea Research Part I: Oceanographic Research Papers*, *45*(2–3), 461–489. https://doi.org/10.1016/s0967-0637(97)00094-0

Yashayaev, I. (2007). Hydrographic changes in the Labrador Sea, 1960–2005. *Progress in Oceanography*, *73*, 242–276. https://doi.org/10.1016/j.pocean.2007.04.015

Yashayaev, I., & Loder, J. W. (2016). Recurrent replenishment of Labrador Sea Water and associated decadal-scale variability. *Journal of Geophysical Research: Oceans*, *121*, 8095–8114. https://doi.org/10.1002/2016jc012046

Zunino, P., Lherminier, P., Mercier, H., Daniault, N., García-Ibáñez, M. I., & Pérez, F. F. (2017). The GEOVIDE cruise in May–June 2014 reveals an intense Meridional Overturning Circulation over a cold and fresh subpolar North Atlantic. *Biogeosciences*, *14*(23), 5323–5342. https://doi.org/10.5194/bg-14-5323-2017